Special Collection

Optimising Adsorptive Stripping Voltammetry: Strategies and Limitations

Yuanzhe Wang, Archana Kaliyaraj Selva Kumar, and Richard G. Compton*[a]

The widely employed electroanalytical technique of adsorptive stripping voltammetry (AdsSV) is critically assessed and evaluated at a wide and diverse range of unmodified and nano-particle modified carbon electrodes using the analyte fipronil as a paradigmatic case. The generic electroanalytical performances of the nano-particle modified electrodes are investigated and compared with the unmodified electrodes revealing similar LOD values and pointing to intrinsic limitations of AdsSV arising from the non-independence of the Faradaic and capacitive signals during the stripping step. Methods for facilitating the adsorption or using different waveforms that may offer a more favourable limit of detection (LOD) at the nano-particle modified electrodes are suggested and assessed, specifically the use of adsorption onto particles *prior* to their use for modifying electrodes and also the recently introduced method of semi-circular voltammetry.

1. Introduction

Stripping voltammetry is a widely adopted strategy in electro-analysis since it offers the opportunity to enhance the sensitivity of the electrochemical method and to reach lower limits of detection than those direct forms of voltammetry where the size of the analytical signal is inevitably limited by the rate of diffusion to the electrode.[2] The constraint created by diffusional rate limitation imposes rather severe generic limitations on direct voltammetry such as linear sweep and cyclic voltammetry as well as, ultimately, the various forms involving pulses and waves.[3] This can be partly moderated by the use of microelectrodes[4] and their arrays[5] but invariably diffusion provides a fundamental rate determining limitation constraining sensitivity.

The attraction of stripping voltammetry is that the analyte is pre-concentrated, including from ultra-dilute solutions below the detection range for direct voltammetry, onto the electrode surface prior to electrochemical analysis in the form of a potential sweep (linear or pulsed) in which a Faradaic current is passed as a result of the oxidation or reduction of the accumulated analyte. By prolonging the period of accumulation the limit of detection (LOD) can in favourable cases be suitably shrunk to meet the stringent demands of certain analytical challenges including the detection of manganese in tea,[6] lead in petrol,[7] and cadmium in blood.[8]

Stripping voltammetry comes in four forms of which anodic and cathodic stripping voltammetry (ASV and CSV) are the most familiar and where a Faradaic reaction is used to realise the pre-concentration step, for example by the reduction of Pb (II) to metallic Pb in the case of ASV[7,9] or its oxidation to PbO_2 in CSV.[10] These chemical processes are reversed during a linear potential sweep which either oxidises the Pb or reduces the PbO_2. A third type of SV is the recently introduced insertive stripping voltammetry,[11] whilst the topic of this paper is to explore the limitations of adsorptive stripping voltammetry (AdsSV).

In AdsSV, as the name suggests, pre-concentration occurs via adsorption onto the electrode surface. This may take place directly onto an electrode, for example, a mercury surface as in the AdsSV analysis of vanadium[12] or onto a modified electrode in which a convenient and attractive electrode, frequently carbon of some form, is supplemented by the addition of a surface layer designed to enhance adsorption so ideally promoting analysis via AdsSV. The surface modification may take the form of a chemisorbed monolayer, a polymeric layer, or as considered in this paper a layer of bespoke particles. In the case of particle modified electrodes (PMEs) a huge diversity of materials has been used including carbon nanotubes,[13] carbon black,[14] TiO_2 nanoparticles[15] and metal (Au, Ag, Pt *etc.*) nanoparticles.[16] We have shown elsewhere[17] that the requirements for the modification are rather stringent unless the particles form a conducting layer since if the binding of the analyte with the modifying particles is too weak then little signal enhancement is seen, but if the interaction is too strong then the analyte is not released sufficiently quickly to usefully benefit the analysis. Even with optimised absorption the merits of the approach can be limited to less than an order of magnitude improvement in analytical signals.[26]

In the present paper we consider the limitations of AdsSV with electrically conducting particle layers from a different perspective, namely to address the question as to what extent

[a] *Y. Wang, A. K. S. Kumar, R. G. Compton*
Department of Chemistry, Physical and Theoretical Chemistry Laboratory
Oxford University
South Parks Road, Oxford OX1 3QZ, UK
E-mail: yuanzhe.wang@wadham.ox.ac.uk
archana.kaliyarajselvakumar@pmb.ox.ac.uk
richard.compton@chem.ox.ac.uk

Supporting information for this article is available on the WWW under https://doi.org/10.1002/celc.202100679

An invited contribution to the Wolfgang Schuhmann Festschrift

the *quantity* of material absorbed influences the analytical signal. This is an easily controllable variable in the design of PMEs via simply changing the number (or mass) of particles adsorbed on the electrode surface. On first thoughts it is obvious that the Faradaic signal seen on the stripping potential scan will increase with the amount of material adsorbed and that the latter will enhance the voltammetric signal. However ultimately the limit of detection is controlled by the ratio of the Faradaic analytical signal as compared to the background currents flowing during the potential scan in which the adsorbed analyte is oxidised or reduced. These Faradaic currents scale both with the voltage scan rate and with the amount adsorbed. However the amount adsorbed will reflect the surface area of the particles used for the modification. At the same time as the background currents are essentially capacitive they too will scale with both voltage scan rate and with the total particle surface area. Hence it is not obvious that increasing the number of particles modifying the surface is analytically helpful. It is the purpose of this paper to explore if this prediction reflects analytical reality and also to compare different adsorbing surfaces to see the extent to which the inferences are general. Specifically we consider surface modified with particles of carbon nanotubes (CNTs), graphene nano-platelets (GNPs) and of carbon black (CB) as well as unmodified surfaces of glassy carbon (GC), basal place graphite (BPPG) and edge plane graphite (EPPG). In the case of particles such as CNTs we complement the AdsSV data with single entity electrochemical measurements[18] to confirm adsorption and the amount of this on the individual particles used in the PME.

As a model target analyte we consider the molecule fipronil (Scheme 1), a phenyl-pyrazole insecticide used for pest control on crops, household pets and domestic animals.[19] Fipronil and its metabolites display neurotoxicity[20] and potential genotoxicity[21] towards non-target animals including humans.[22] The wide use of fipronil has raised concerns because of the residual fipronil present in soil or aquatic ecosystems[20,23] given its threat to human health.[24] The methods reported for the analysis of fipronil are mostly chromatographic,[25] while recently some cheap and rapid techniques have emerged[26] including a few electrochemical methods.[26c–h] The method we evaluate in the present paper employing AdsSV on the aforementioned carbon electrodes, particularly on a CNT modified surface can be seen in principle as an electroanalytical method alternative to the existing analytical methods for fipronil determination. However the intrinsic limitations of the AdsSV method as evaluated in then following indicates a clear lower limit for electroanalytical detection via this approach; clarifying the reasons for this are the aims of this paper.

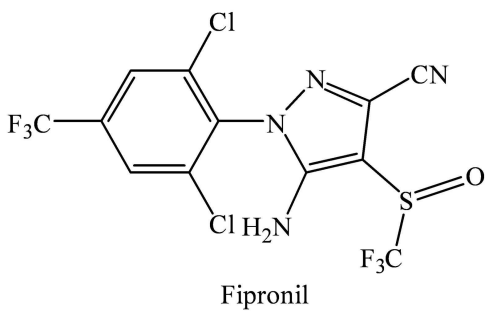

Fipronil

Scheme 1. Structure of Fipronil (5-amino-1-[2,6-dichloro-4-(trifluoromethyl) phenyl]-4-[(trifluoromethyl)sulfinyl]-1H-pyrazole-3-carbonitrile)

Experimental

Chemicals and Apparatus

All chemicals were of analytical grade and were used received without any further purification. Fipronil (FIP, Pantanal®) and methanol (≥99.0% purity) were purchased from Sigma-Aldrich. The bamboo-like multi-walled carbon nanotubes (b-MWCNTs, 30± 10 nm diameter, 5–20 μm length, >95% purity) were purchased from NanoLab, Brighton, MA, USA. Graphene nano-platelets (GNPs, 15 μm in width, 6–8 nm in thickness) with a known average area of 297±152 μm^2 (from scanning electron microscopy[1]) were purchased from Strem Chemicals, MA, USA. Carbon Black (CB, M 1100, Monarch®) was purchased from Cabot Performance, Billerica, MA, USA. All aqueous solutions were prepared with deionised water with a resistivity of 18.2 MΩ cm at 298 K (Millipore, MA, USA). The Britton-Robinson (BR) buffer (0.1 M, pH=8.0) was prepared using sodium hydroxide (97% purity, Sigma-Aldrich), phosphoric acid (99.99% purity, Aldrich), acetic acid (99.5% purity, BDH), boric acid (99.5% purity, Aldrich) and potassium chloride (≥99.0% purity, Sigma-Aldrich). Stock solutions of FIP (5 mM) were prepared by dissolving FIP in methanol. All solutions of required concentrations were prepared freshly every day from the stock solution by dilution with the mixture of 60% B-R buffer (pH 8.0) and 40% methanol.

All electrochemical experiments were performed at 298 K with a standard three-electrode configuration inside a Faraday cage by using an in-lab built potentiostat. As previously described,[27] the potentiostat was software controlled by *Python* 3.5 to generate the required potential waveforms and measurements with low noise and a high sampling rate (100 kHz maximum).

Voltammetry on Carbon Macroelectrodes

For voltammetric experiments, several carbon-based macroelectrodes were used variously as the working electrode. A saturated calomel electrode (SCE, BASi Inc., Japan) was used as the reference electrode and a graphite rod as the counter electrode. The macroelectrodes employed as working electrodes were a glassy carbon (GC) electrode with a diameter of 3.0 mm, a basal plane pyrolytic graphite (BPPG) electrode with a diameter of 4.9 mm, an edge plane pyrolytic graphite (EPPG) with a diameter of 4.3 mm and the same glassy carbon electrode modified with carbon black (CB), multiwalled carbon nanotubes (MWCNTs) or graphene nano-platelets (GNPs).

The GC and EPPG electrodes were polished on the soft lapping pads with alumina of decreasing particle sizes (1.0, 0.3 and 0.05 μm) (Buehler, IL, UK), followed by sonication for 10 s in water. The BPPG electrode surface was prepared by polishing on the sand paper of grade P4000 and then repeatedly for several times pressing on and then removing from the sticky tape, 'cellotape' (Henkel AG, Dusseldorf, Germany), before finally washing with acetone.[28] The CB, MWCNTs and GNPs modified GC electrodes were prepared by a dropcast method. The nanoparticle materials were first dispersed (1 mg/1 mL) in either pure methanol or methanol solutions containing varying concentrations of FIP by sonication for 30 minutes without further functionalisation. 2.5–30 μL of the obtained

suspensions (with or without the modification by FIP) were then dropcasted (in 2.5 μL aliquots) on to the clean GC electrode, followed by solvent evaporation under a gentle N_2 flow.[29]

Cyclic voltammetric experiments were conducted at unmodified GC, BPPG, EPPG or modified GC electrodes in blank solution (the mixture of 60% B-R buffer (pH 8) and 40% methanol) or 0.1 mM FIP solution to investigate the influence of scan rate. Adsorptive stripping voltammetry (AdsSV), adsorptive square wave voltammetry (AdsSWV), adsorptive semi-circular sweep voltammetry (AdsSCV), prior-adsorptive stripping voltammetry (pAdsSV) were conducted in order to understand the adsorption process and assess the detection sensitivity at the carbon-based electrodes. AdsSV, AdsSWV and AdsSCV were conducted by immersing the electrode (unmodified GC, BPPG, EPPG or GC electrode dropcasted with unmodified MWCNTs or GNPs) in the standard solutions of varying concentrations of FIP. The accumulation of FIP onto the electrode surface was performed under open-circuit potential conditions with stirring of the solution for 0–6 minutes. The pAdsSV measurements were made in the blank solution using the GC electrode dropcasted with CB and GNPs pre-modified by FIP.

Nano-impact Experiments

Nano-impact experiments were conducted by measuring the chronoamperometry at a carbon fibre wire microelectrode system using the same reference and counter electrode as above. Note the potentiostat used in this work ensures an accurate conservation of the charge transferred during a particle-impact event.[18b] The carbon fibre wire microelectrode was fabricated from a carbon fibre (diameter 7.0 μm, Goodfellow, Cambridge, UK) following the procedure introduced previously.[30] The length of the microelectrode was 1 mm. 10 μL of MWCNT suspension prepared as described in 2.2 was added to 10 mL of the blank solution or the 0.1 mM FIP solution, followed immediately by a chronoamperometric measurement. The chronoamperograms were recorded for 20 s at varying potentials from 0.8–1.7 V vs SCE.

2. Results and Discussion

In the following sections, first, adsorptive stripping voltammetry (AdsSV) or, novelly, prior-adsorptive stripping voltammetry (pAdsSV) is applied to examine the electrochemical signals of fipronil (FIP) at six types of carbon electrode surfaces. The adsorption of FIP on glassy carbon (GC), basal plane pyrolytic graphite (BPPG), edge plane pyrolytic graphite (EPPG), multi-walled carbon nanotubes (MWCNTs) and graphene nanoplatelets (GNPs) surfaces are investigated and characterised. Next, the adsorption of FIP on single MWCNTs is investigated via nano-impacts. Finally, in the last section, the electroanalytical performances of AdsSV on these five carbon electrode surfaces are compared. The effects of the types and the amounts of carbon materials on the detection limit are demonstrated, then, in combination with the results obtained in the previous two sections, explanations are offered for the presented merits and limitations of employing AdsSV at the unmodified and nanoparticle modified surfaces. Also in this section, electroanalysis of FIP using adsorptive square wave (AdsSWV) and adsorptive semi-circular sweep voltammetry (AdsSCV) is evaluated at optimised MWCNT electrode surfaces.

2.1. Electrochemical Behaviour of Fipronil

The voltammetric responses of the FIP in a mixture of 60% pH 8.0 B-R buffer and 40% methanol were first explored at all carbon surfaces of interest. Figure 1 depicts the cyclic voltammetric responses of the 0.1 mM FIP solution obtained at the unmodified GC, EPPG and BPPG electrodes overlaid with those obtained at CB, GNP and MWCNT modified GC electrodes. The masses of MWCNTs, GNPs and CBs dropcasted on the GC electrode was 10 μg, 10 μg and 25 μg, respectively. The voltammetric responses at the electrode modified with other amounts of MWCNTs and GNPs are shown and discussed in section 3.3. The unmodified GC, EPPG, BPPG electrode and MWCNT modified GC electrode were immersed in the 100 μM FIP solution under open circuit conditions for an optimised accumulation time of 2 minutes (see Figure S1 for the optimisation) and subsequently the voltammetric responses were recorded. The adsorption of FIP on GNPs and CB were facilitated via immersion in a 100 μM FIP methanol solution prior to dropcasting. The voltammetry at the electrode dropcasted with GNPs or CB was then recorded in a blank solution. This method used for GNPs and CB modified GC electrodes is introduced here as pAdsSV. In this method, thought to be novel, the modifying particles are saturated with the adsorbate *prior* to drop casting in contrast to the usual method in which the sequence is reversed, namely drop-casting followed by transfer of the electrode to the analyte solution for analysis. We label this approach pAdsSV and have found it helpful in minimising loss of particles from the electrode surface if long times are needed for accumulation. This technique was applied to enable a maximum adsorption of analyte to the electrode surface and hence boost the sensitivity of detection. This will be further demonstrated and discussed in section 3.3. The voltammograms were recorded using a slow scan rate of 5 mVs^{-1} to attain a favourable resolution of signals particularly for the nanoparticle modified electrode surfaces. As shown in Figure 1,

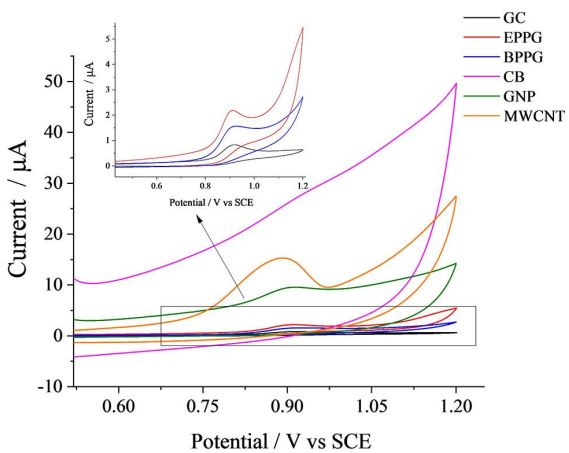

Figure 1. The adsorptive stripping cyclic voltammetric responses of 0.1 mM FIP on unmodified GC, BPPG, EPPG, CB modified GC, GNPs modified GC and MWCNTs modified GC electrode in a mixture of 40% methanol and 60% PH 8 B-R buffer. The voltammograms were either recorded after a 2-mintue open circuit accumulation or a dropcast of nanoparticle materials modified with FIP at the scan rate of 5 mV/s.

oxidation peaks were observed at similar potentials at all carbon surfaces, which are 0.92 V vs SCE for GC and BPPG, 0.91 V vs SCE for EPPG and GNP and 0.89 V vs SCE for MWCNT surface. No FIP related signal was seen on CB modified electrodes. This likely reflects structural differences between CB and the graphitic forms of carbon[31] leading to negligible adsorption on CB where graphitic planes are absent. CB was not investigated further.

Next to further study the adsorptions of FIP onto the electrode surfaces, the effect of scan rate was investigated at the unmodified GC, BPPG and EPPG electrode, as well as the MWCNT and GNP modified GC electrodes using the stripping voltammetry analytical procedures as described above. The results are shown in Figure S2–S6 in the SI. The peak currents are linear with scan rate and the slopes of the corresponding log-log plots were close to 1 at the five surfaces in the low scan rate ranges, suggesting the oxidation processes of FIP are surface controlled. The oxidation is suggested to correspond to a two-electron transfer process generating fipronil-sulfone[26c] (structure shown in Figure S7), which is a well-recognised oxidative degradation product of FIP.[32].

Having identified the surface-bound nature of the FIP oxidation processes, the adsorptions of FIP on the five carbon surfaces were next characterised by considering the possible approximate applicability of the Langmuir isotherm:[33]

$$\theta = \frac{K[FIP]}{1 + K[FIP]} \quad (1)$$

where θ is the fractional occupancy of the adsorption sites, K is the equilibrium constant for adsorption and *[FIP]* is the concentration of FIP. Eq. (1) can be re-written as:

$$\frac{1}{Q} = \left(\frac{1}{KQ_{max}}\right)\left(\frac{1}{[FIP]}\right) + \frac{1}{Q_{max}} \quad (2)$$

where Q is the voltammetrically measured charge transferred during oxidation of the species at the studied concentrations. Q_{max} is maximum charge transfer at the surface saturated with FIP. Voltammetric responses at the GC, BPPG, EPPG, MWCNT and GNP surfaces were recorded in varying concentrations of FIP solutions using the same procedure as above. Figure 2 shows an example of Langmuir plot obtained from the voltammograms of 5–200 μM FIP recorded at the MWCNT modified GC electrode (shown in the inset of Figure 2). Linearity ($(1/Q\ \ (\mu C^{-1}) = (0.22 \pm 0.0070)\ \ 1/C\ \ (\mu M^{-1}) + (0.0018 \pm 0.000067)$, $R^2 = 0.996$) was found in the double reciprocal plot, as predicted by the Langmuir isotherm. Thus K and Q_{max} were determined according to Eq. (2) as $(8.2 \pm 0.3) \times 10^{-3}$ $\mu m^{-1}$and (546 ± 20.3) μC, respectively. Similarly Q_{max} was determined for the other four carbon surfaces where similar linearity was observed. In comparison to the unmodified surfaces, the Q_{max} obtained at the particle modified electrode surfaces are significantly larger due to the much increased adsorption (Figure S8). In all cases the data were not inconsistent with the Langmuir isotherm.

The theoretical area per FIP molecule, A_{FIP} was estimated using a simple 'rectangular box model'[34] as presented in

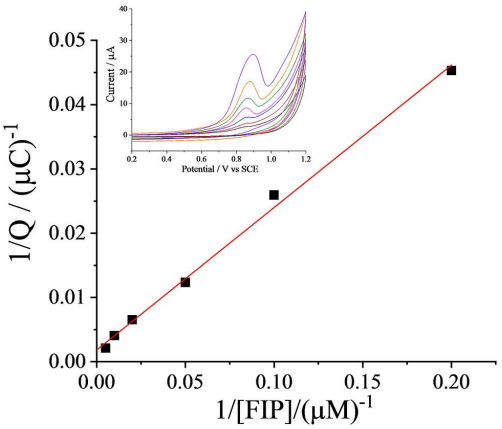

Figure 2. The plot of *1/Q* against *1/C* where the peak area values obtained from the adsorptive stripping voltammograms of 5–200 μM FIP at MWCNTs modified GC (inset). The peak areas were analysed by subtracting an 8th order polynomial fitted baseline from the original voltammograms.

Scheme 2. The dimensions of the molecule are shown in all three possible flat molecular orientations. All side lengths were estimated by trigonometry using bond lengths, bond angles and the van der Waals radii of the terminating atoms. The bond length, bond angles data were obtained from ChemDraw 16.0 software. The van der Waals radii of the terminating atoms values are those tabulated by Rowland.[35] The areas corresponding to the adsorption of FIP in flat (A), edgewise (B) and endwise (C) orientations A_{fl}, A_{ed} and A_{en} were estimated as 14×10^{-15} cm^2, 12.5×10^{-15} cm^2 and 7×10^{-15} cm^2 respectively. Assuming close-packed, monolayer adsorption of FIP and the number of electron transferred (n) is 2, the number of molecules adsorbed on electrode surfaces (N_{ads}) can be thus determined from Q and the electron fundamental charge e (1.602×10^{-19} C) by $N_{ads} = Q/(ne)$. Accordingly the "real" surface area of the electrode, $A_{electrode}$, available for adsorption of FIP, can be estimated using N_{ads} and A_{FIP} by $A_{electrode} = N_{ads} \times A_{FIP}$. Table 1 lists the values of the charge transfer occurring in

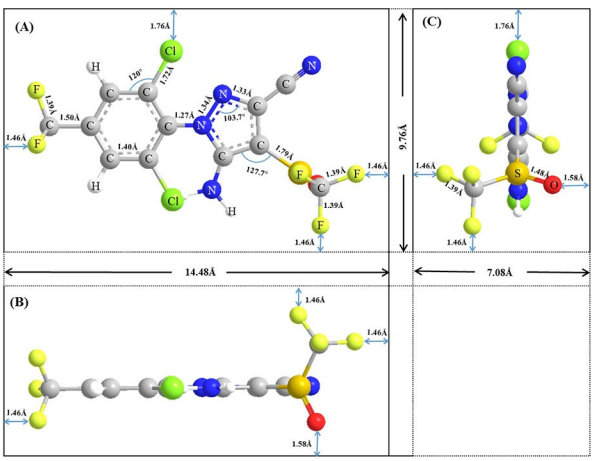

Scheme 2. Rectangular box model of FIP molecule: (A) flat view, (B) edgewise view and (C) endwise view

Table 1. The charge, geometric or characterised areas electro-active areas found in the 0.1 mM FIP solution for GC, BPPG, EPPG, MWCNT, GNP surfaces.

Surface	Q_0 [μC]	Geometric or characterised area [cm^2]	Electro-active area [cm^2] assuming the molecule landed with the side of: flat view (A)	Edgewise view (B)	Endwise view (C)
GC	8.83	7.07×10^{-2}	39×10^{-2}	34×10^{-2}	19×10^{-2}
BPPG	19.9	18.9×10^{-2}	88×10^{-2}	78×10^{-2}	43×10^{-2}
EPPG	18.2	14.5×10^{-2}	80×10^{-2}	71×10^{-2}	40×10^{-2}
MWCNT	246	20–40[a]	11	10	5
GNP	42.2	6.2 ± 3.2[b]	1.9	1.6	0.9

[a] The value was calculated from the specific surface area provided by the supplier NanoLab; [b] The value was estimated using SEM,[1] see Section 5 of SI for the calculation.

0.1 mM FIP solution, Q_0 and the area, $A_{electrode}$ obtained for the five studied surfaces as well as the geometric areas of the three unmodified electrodes and the surface areas of the two modified electrodes characterised by the supplier and an independent SEM study.[1] As can be seen in Table 1, the electro-active surface areas of the unmodified electrodes were approximately 2.3–5.5 times of the geometric areas. Under the aforementioned assumption of monolayer adsorption this suggests a considerable contribution from the roughness of theses surfaces. In fact the roughness factor for GC electrodes is reported as lying in the range 1.7–4.1[36] High roughness levels of pyrolytic graphite electrode surfaces have also been noted.[37] However for the nano-entity modified electrode surfaces, the electro-active area values indicates likely sub-monolayer adsorption at both GNP and MWCNT surfaces. The low levels of adsorptions are possibly caused by desorption[34a] of FIP and/or the aggregation/agglomeration of the dropcasted MWCNTs leading to the reduced surface accessibility. To further investigate this and to assess the potential of improving the detection sensitivity the single entity electrochemistry of MWCNT was studied as an example in the next section.

2.2. Adsorption on Single Carbon Nanotubes: A Nano-impact Study

The oxidation of FIP on individual MWCNTs was investigated using the nano-impact method. 10 μL of a MWCNT in methanol suspension was added to 10 mL of a solution of 60% pH 8.0 B-R buffer and 40% methanol containing 0.1 mM FIP and was left for 5 minutes allowing for the adsorption of FIP. A fresh carbon fibre electrode was immersed in the new suspension and chronoamperograms were immediately recorded with the potential held at a value in the range 0.8–1.7 V vs SCE for the duration of 20 seconds. Chronoamperograms were also recorded at the same potentials in the same FIP solution but without the presence of MWCNTs and in the suspension of the same amount of MWCNTs in the blank solution without the presence of FIP. As shown in the representative chronoamperograms in Figure 3(A), large oxidative spikes (of average duration (7.6 ± 3.3) s) were observed for the suspensions of MWCNTs in the presence of FIP and inferred to be Faradaic. Much smaller spikes (of average duration (4.7 ± 2.2) s) were observed in the absence of MWCNTs and were inferred to be capacitive (see below). Each spike corresponds to a collision of an individual MWCNT with the micro-electrode as a result of the Brownian motion of the MWCNTs.[18b,c] This was confirmed by the chronoamperogram recorded in the 0.1 mM FIP solution at the same potential of 1.6 V SCE in the absence of MWCNTs where no spikes were detected (Figure S9). The average charge passed per spike were obtained from averaging the integration of each single-peaked, sharp shaped spike for each potential (Figure 3(B)). The 'quasi-step' like impacts and the multi-peaked spikes were excluded since they may likely be the results of simultaneous collisions of aggregated MWCNTs or arise from the adsorption onto the electrode of the MWCNTs as has been noted in other solvents.[38] As revealed by Figure 3(B), the average charges measured for the spikes detected in the MWCNTs-FIP suspension are very significantly larger than those detected in the blank MWNCT suspension and increase to a limiting value with the increase of potential particularly in the range of 1.1–1.5 V SCE consistent with the Faradaic oxidation of FIP. As established previously the spikes may result from the Faradaic and/or the capacitive charge transfer process occurring during the collision between the nano-particles and microelectrode.[1,18b] The Faradaic charge transferred during the impact timescale increases substantially when an over-potential enabling the redox reaction to proceed is applied, which is consistent with the case observed for MWCNTs-FIP suspension. In contrast the small spikes detected in the blank MWCNT suspension show a small and potential insensitive magnitude over the whole potential range, as shown in Figure 3(B), indicating the sole contribution is from the capacitive charge transfer at electrode-electrolyte interface taking place when the applied potential deviates from the potential of zero charge.[1,39]

Chronoamperograms at 1.6 V vs SCE were analysed where the average charge per Faradaic spike reaches a plateau (see Figure 3(B)) and the Faradaic oxidation of FIP was thought complete. A total number of 106 single-peaked, sharp-shaped spikes were collected from eight independent chronoamperograms. As the capacitative charge transferred is negligible, the measured charge transferred per spike can be approximated to the charge transferred in the electro-oxidation of the FIP at a single MWCNT. Figure 3(B) shows the charge distribution of the collected spikes assuming a uniform adsorption reflects the surface area distribution of the individual MWCNTs present in the suspension. Using the equations described in section 3.1, the surface area of a single MWCNT can be estimated from the charge passed per spike and the area per FIP molecule assuming monolayer close-packed coverage.

The average charge of the collected spikes is (2.82 ± 0.34) μA (standard error applied), from which the mean surface area of single MWCNT was calculated as (12.4 ± 1.5), (11.0 ± 1.3) or (6.1 ± 0.73) μm^2 which correspond to the adsorption via flat, edgewise, endwise orientation, respectively (see section 5 of the SI for detailed calculations). The electro-active surface area obtained from nano-impacts lies approximately in the same

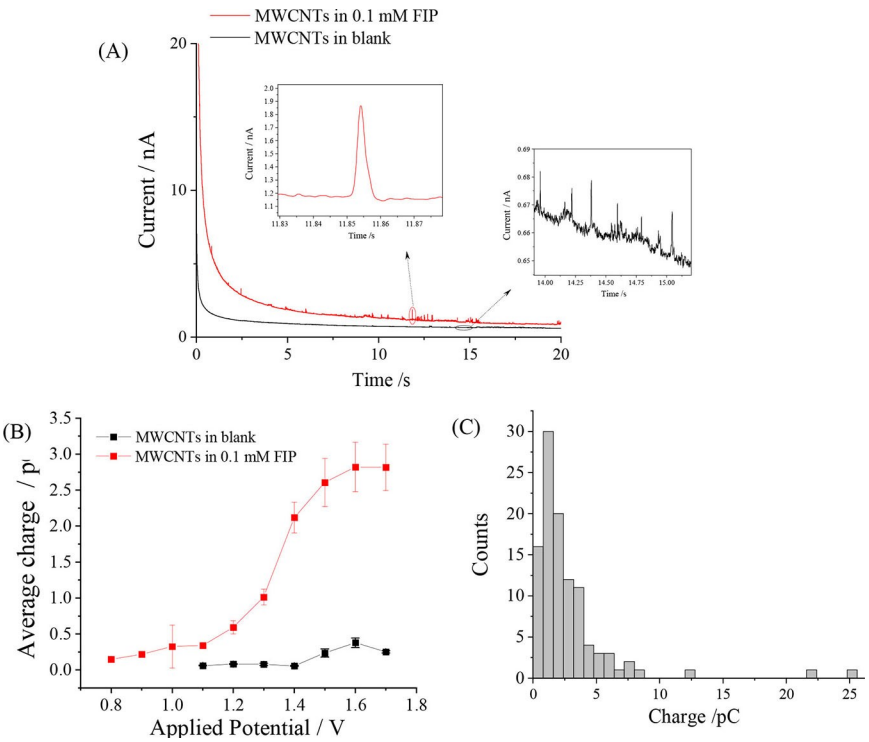

Figure 3. (A) Representative chronoamperogram recorded at 1.6 V vs SCE with the presence and absence of 0.1 mM FIP in a 10 μg MWCNT suspension for the duration of 20 seconds. The enlarged graphs show the oxidative spikes resulting from FIP oxidation (red) and the capacitive spikes (black). (B) The average charge transferred per spike at varying potentials of 0.8–1.7 V vs SCE. No spikes were detected in the blank MWCNT suspension at potentials lower than 1.1 V vs SCE. The error bars are the standard error bar which defined by $SD/(n)^{1/2}$, where SD is the standard deviation and n is the number of the spikes at each potential. (C) The charge distribution of the 106 spikes detected at 1.6 V SCE.

range with the specific surface area estimated from the supplier's data (4–9 μm^2), suggesting the adsorption of FIP on a single MWCNT is monolayer in extent.

In comparison to the sub-monolayer coverage estimated for the dropcasted MWCNTs immersing in the same concentration of FIP solution, the coverage on the dispersed MWCNTs is distinctly higher and limits (Figure 3(B)) at the monolayer. Thus the impact experiments confirm that FIP molecule adsorbed onto MWCNTs in a monolayer manner and hence that adsorption is partially diminished in the case of MWCNT dropcast layers where aggregation/agglomeration of the nanotubes may operate to the detriment of full adsorption.

2.3. Analytical Performance of Different Carbon Electrode Surfaces

First the analytical responses of FIP at the particle modified electrodes (PME) and the unmodified GC, BPPG and EPPG electrodes were compared. Figure 4(A)–(D) depict the background-subtracted adsorptive stripping voltammetric responses of varying concentrations of FIP in 60% pH 8 B-R buffer and 40% methanol at GC, BPPG, EPPG and MWCNTs modified GC electrodes. Peak area (charge) rather than peak height was chosen as it is the more robust analytical parameter in comparison to the latter for measuring the peak sizes in the baseline-subtracted voltammograms. The stripping charges were obtained from integration of the oxidation peaks shown in Figure 4(A)–(D) and were linear with concentrations in the ranges of 3–20 μM at both the GC and BPPG electrode, 5–40 μM at the EPPG electrode and 2.5–20 μM at the MWCNTs modified electrode. As can be seen, the oxidation peak with the largest magnitude was found at the MWCNTs modified GC electrode, where the obtained charge is ca. 16 times larger in comparison with which found at the unmodified GC. However, the linear ranges were very similar to those found at the unmodified electrodes and the detection limit was obtained as 2.5 μM at the MWCNTs modified GC electrode, which is not significantly lower than the detection limits at the unmodified GC (3 μM), BPPG (3 μM) and EPPG (5 μM) electrodes.

Figure 4(E)–(G) compare the voltammetric performances at the GNP modified GC electrode recorded using the suggested novel pAdsSV (Figure 4(E)) to those using conventional AdsSV which involves immersing the electrode dropcasted with the unmodified GNPs in varying concentrations of FIP under open circuit condition for 2 minutes (Figure 4(F)). It is shown clearly by Figure 5(G) that the pAdsSV resulted in greater signals and lower detection limit. The advantage of employing pAdsSV at GNPs modified GC electrode over AdsSV js thus demonstrated. Using the more sensitive pAdsSV, the linear detection range at the GNPs modified GC electrode was found to shift to the higher concentrations of 30–500 μM.

Next, to better understand the factors contributing to the differences and similarities in the observed signal sizes and the

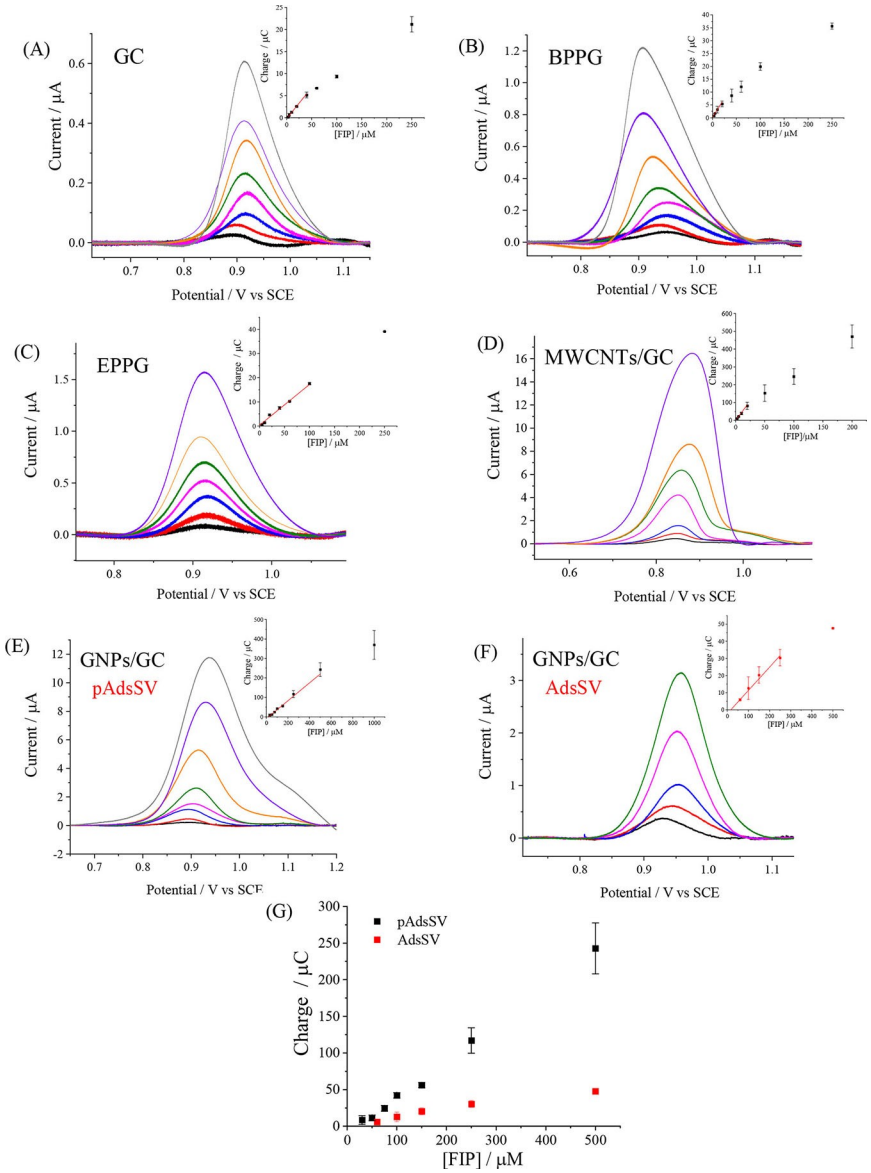

Figure 4. The adsorptive stripping voltammetric responses of varying concentrations of FIP recorded after a 2-mintue open circuit accumulation at (A) unmodified GC, (B) BPPG, (C) EPPG, (D) 10 µg MWCNTs modified GC (MWCNTs/GC) and (E) 10 µg GNPs modified GC electrode (GNPs/GC) or recorded at (F) the GC electrode dropcasted with 10 µg FIP-modified GNPs at the scan rate of 5 mV/s. The shown voltammograms were subtracted with an 8th order polynomial fitted baseline. The plots of charge versus concentration were shown in the insets and (G), where the charge was obtained from the three repeating voltammetric measurements.

detection limits at different electrode surfaces, the capacitances of each electrode were considered. The capacitance describes the double-layer charging at the electrode- solution interface and, if constant, is related to the electrode surface area by:[40]

$$\Delta I = 2ACv \quad (3)$$

where ΔI is the difference between the measured forward and backward current, A is the effective surface area, C is the capacitance per unit area and v is the scan rate. Using Eq. (3) the capacitances can be determined from the cyclic voltammograms measured in the blank solution of 60% B-R buffer and 40% methanol at GC, BPPG, EPPG, MWCNTs and GNPs modified GC electrode. For each electrode, varying scan rates were applied and linear plots of ΔI (read at the potential of 0.5 V vs SCE) versus v were obtained, from the slope of the plots the capacitances at 0.5 V vs SCE can be calculated (see Figure S10). Table 2 lists the overall capacitance and the specific capacitance of each electrode estimated using the electroactive surface areas and characterised surface areas shown in Table 1 for unmodified electrodes and PMEs, respectively. It can be seen in Table 2 that the overall capacitances which are controlled by the surface areas are much smaller for unmodified electrodes in comparison to the PMEs. The specific capacitances of all studied carbon surfaces lie in the similar ranges of 5.3–64.3 µF/cm^2, close to the typical double-layer capacitance

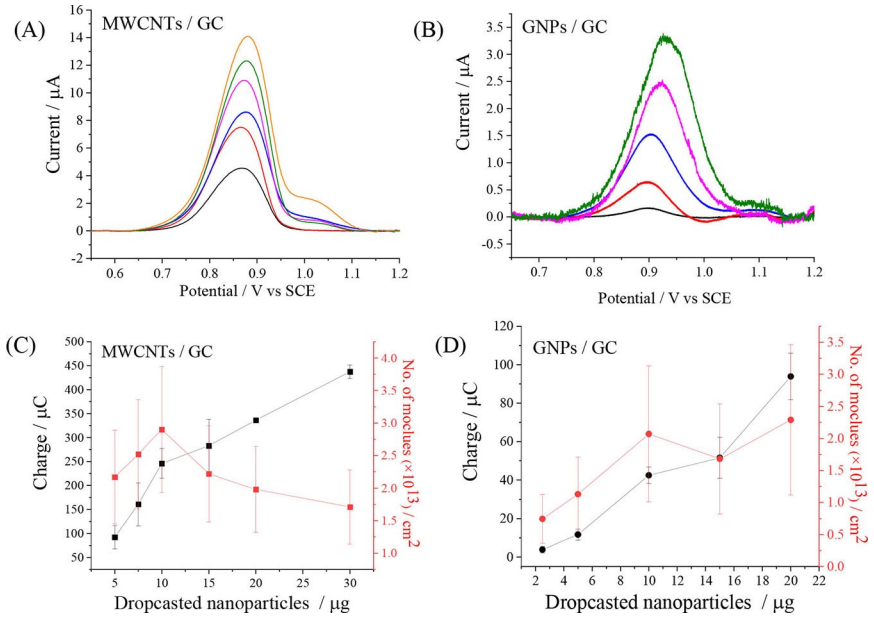

Figure 5. The background-subtracted adsorptive stripping voltammetric responses of 0.1 mM FIP at (A) 5, 7.5, 10, 15,20 and 30 µg MWCNTs modified GC and (B) 2.5, 5, 10, 15 and 20 µg GNPs modified GC electrode. The relations of charges and the surface coverage (in number of molecules per unit) obtained from oxidation peak in (A) and (B) were plotted in (C) and (D), respectively.

Table 2. Summary of capacitances, specific capacitances, the lowest detectable concentrations and the signal to background ratios in the voltammograms of the lowest detectable concentration of the studied electrode surfaces. The ranges shown for the specific capacitance reflect both the ranges of the surface areas and the standard deviations of the estimated capacitances.

Electrode	Overall capacitance [µF]	Specific capacitance [µF cm^{-2}]	Signal to background ratio	LOD [µM]
GC	7.8 ± 0.24	20–42	0.10	3
BPPG	9.6 ± 0.08	11–22	0.15	3
EPPG	25 ± 0.33	31–64	0.095	5
MWCNTs/GC	210 ± 3.4	5.3–11	0.10	2.5
GNPs/GC	210 ± 6.0	34 ± 17	0.025	60

values.[40–41] Note that unlike true capacitors, the double layer capacitance is often dependent on the potentials applied.[40]

Table 2 also summarises the lowest detected concentration of FIP at each electrode and the signal to background ratios of the peaks current read from the lowest concentration voltammograms shown in Figure 4(A)–(E) and the capacitative currents read at the same potentials Figure S10. The signal to background ratio reflects the relation of the aforementioned

capacitative charge and the stripping charge associated with the amounts of electro-active adsorbate present. As suggested by Table 2 the signal to background ratios values of three unmodified electrodes and the MWCNTs modified GC electrode are similar and are larger than the GNPs modified GC electrode. This pattern was also observed for LOD and hence it can be concluded that the LOD is dependent on the signal-background ratio rather than solely the magnitude of signal. Thus despite the fact that larger signals were seen at the PMEs with larger surface areas, the LODs of AdsSV are also affected by proportionally larger capacitances presented and are intrinsically limited by an upper limit of monolayer adsorption, as discussed in section 3.2.

Having compared the different types of carbon materials, we next focus on the PMEs and investigate the effect of the amounts of nano-particles used for modifying the electrode. Figure 5(A) and 5(B) show the background-subtracted AdsSV voltammograms of 0.1 mM FIP recorded at a GC electrode modified with either 5–30 µg of MWCNTs or 2.5–20 µg of following the procedures described in section 3.1. Figures 5(C) and 5(D) plot the charges (*Q*) and the surface coverages (number of molecules absorbed on per unit area) of FIP on the nano-particle surfaces. The latter were estimated by $N_{ads}/A_{electrode}$, where N_{ads} was the total number of molecules adsorbed on electrode surfaces calculated from *Q* as described in section 3.1 and $A_{electrode}$ was the surface area of varying mass of MWCNTs and GNPs calculated in SI, section 5. As suggested in Figure 5(C) and 5(D), the oxidative charge broadly increased with the amount of nano-particles dropcasted but the charge per unit area of adsorbing surface remained approximately constant. The former was again owing to the larger surface areas of the nanoparticles used, which was evidenced by the voltammograms measured at the electrodes modified with the same amounts of MWCNTs and GNPs in the blank solution (see Figure S11), where the capacitative currents scaled with the increasing amounts of MWCNTs and GNPs.

From the discussions earlier in this section increasing the amount of particles on the surface also increases the capacitive signals and using a larger surface area is unable to enhance the LOD unless the adsorption per unit area is also boosted. For the subsequent analytical studies using either MWCNTs and GNPs, 10 µg was chosen as the mass for the preparation of the PMEs.

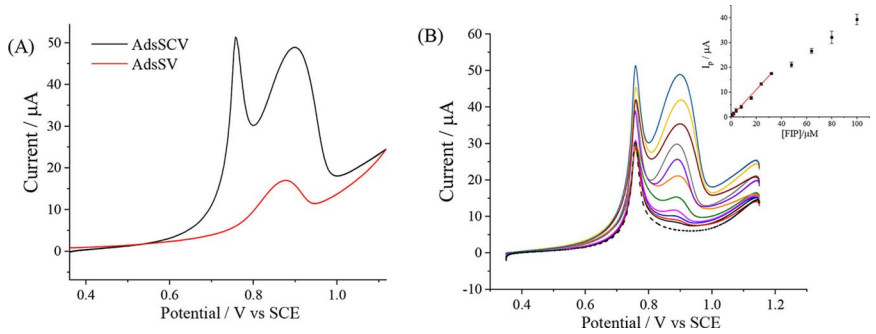

Figure 6. The adsorptive semi-circular sweep voltammetric responses at the MWCNTs modified GC electrode using a potential window with E_{mid} of 0.75 V vs SCE and the scan amplitude of 0.4 V of (A) 100 µM FIP solution overlaid with the adsorptive linear sweep voltammetric response at the same average scan rate of 5 mV/s and (B) 0 to 100 µM of FIP solutions. Inset of (B): The obtained peak currents with the subtraction of the value read at 0.90 V vs SCE of the blank solution voltammogram (dash line) -WRONG POSITION! Not embedded in the main body of article

Finally the possibility of further improving the limit and sensitivity of detection by employing the voltammetric techniques with different potential waveforms was examined at the optimised MWCNTs modified GC electrode surface where a relatively favourable analytical performance using AdsSV was observed. The commonly used adsorptive square wave voltammetry, AdsSWV, was first attempted however, the signal was lost in the voltammograms (see Figure S12 for the example voltammogram) since the backward and forward signals were found to cancel out. The forward scans was recorded in varying concentrations of FIP solutions and the LOD was found to be 4 µM (Figure S13).

Next we turned to the recently advocated semi-circular potential sweep voltammetry (SCV) but, novelly, with a preconcentration step applied, AdsSCV. The SCV technique was reported in our previous work.[42] Briefly, the scan rate varies over the potential window generated by a semi-circular potential wave function. The midpoint of the potential window (E_{mid}) can be adjusted to approximate the redox potential where the scan rate reaches a near infinite value and the present signals are greatly amplified. Here the E_{mid} was optimised as 0.75 V vs SCE (Figure S14) and the resulting adsorptive semi-circular voltammetric response of 0.1 mM FIP was compared with the adsorptive linear sweep voltammetric response in Figure 6(A). The voltammograms of varying concentrations of FIP solutions ranging from 0 to 100 µM obtained using AdsSCV are shown in Figure 6(B) and the linear detection range was found to be 1–32 µM. The LOD obtained using AdsSCV was 1 µM, which is somewhat but not substantially lower in comparison to using the other two conventional electroanalytical techniques (4 µM for the forward scan of AdsSWV and 2.5 µM for the linear sweep AdsSV).

3. Conclusions

This work demonstrates the limitations and optimising strategies of the electroanalytical detection using adsorptive stripping voltammetry for the model molecule FIP so as to give generic insights. The adsorption of FIP at the unmodified electrodes (GC, BPPG EPPG electrode) and the PMEs (MWCNTs and GNPs modified GC electrode) was evidenced and characterised using the voltammetric studies and via nano-impact experiments at the single MWCNT surface. The adsorptions were identified to be no more than mono-layer for all the studied electrode surfaces. This intrinsically limits the LODs reflected by the signal to background ratios. The PMEs shows no obvious advantage in comparison to the unmodified electrodes in terms of improving the LOD despite larger signals are detected since an increased area for adsorption is offset by an increased capacitive charging signal. Nonetheless two strategies were developed for PMEs to enhance the analytical performance, specifically the use of pAdsSV technique facilitating the adsorption of FIP at GNPs modified GC electrode and the use of AdsSCV technique at MWCNTs modified GC electrode which selectively amplifies the signal and results in the low LOD.

Acknowledgements

Archana K S thanks the Commonwealth Scholarship Commissions, UK for funding her DPhil research at the University of Oxford.

Conflict of Interest

The authors declare no conflict of interest.

Keywords: adsorptive striping voltammetry · adsorption · nanoparticles · nano-impact · electroanalytical chemistry

[1] J. Poon, C. Batchelor-McAuley, K. Tschulik, R. G. Compton, *C* **2015**, *6*, 2869–2876.
[2] a) J. Wang, *Analytical electrochemistry*, 3rd ed., Wiley-VCH, Hoboken, N. J., **2006**; b) C. M. A. Brett, A. M. O. Brett, *Electrochemistry: principles, methods, and applications*, Oxford University Press, Oxford, **1993**.
[3] Á. Molina, J. González, *Pulse voltammetry in physical electrochemistry and electroanalysis: theory and applications*, 1st ed., Springer, **2016**.
[4] M. Fleischmann, S. Pons, *Anal. Chem.* **1987**, *59*, 1391A-1399A.
[5] a) H. P. Wu, *Anal. Chem.* **1993**, *65*, 1643–1646; b) L. J. Magee, J. Osteryoung, *Anal. Chem.* **1989**, *61*, 2124–2126; c) R. G. Compton, G. G.

Wildgoose, N. V. Rees, I. Streeter, R. Baron, *Chem. Phys. Lett.* **2008**, *459*, 1–17.
[6] A. J. Saterlay, J. S. Foord, R. G. Compton, *Analyst* **1999**, *124*, 1791–1796.
[7] A. N. Blythe, R. P. Akkermans, R. G. Compton, *Electroanalysis* **2000**, *12*, 16–20.
[8] J. Kruusma, L. Nei, J. L. Hardcastle, R. G. Compton, E. Lust, H. Keis, *Electroanalysis* **2004**, *16*, 399–403.
[9] C. Prado, S. J. Wilkins, F. Marken, R. G. Compton, *Electroanalysis* **2002**, *14*, 262–272.
[10] A. J. Saterlay, C. Agra-Gutiérrez, M. P. Taylor, F. Marken, R. G. Compton, *Electroanalysis* **1999**, *11*, 1083–1088.
[11] a) A. L. Suherman, M. Lin, B. Rasche, R. G. Compton, *ACS Sens.* **2020**, *5*, 519–526; b) A. L. Suherman, B. Rasche, B. Godlewska, P. Nicholas, S. Herlihy, N. Caiger, P. J. Cowen, R. G. Compton, *ACS Sens.* **2019**, *4*, 2497–2506.
[12] C. Agra-Gutiérrez, R. G. Compton, *Electroanalysis* **1998**, *10*, 204–206.
[13] a) M. C. Henstridge, E. J. F. Dickinson, M. Aslanoglu, C. Batchelor-McAuley, R. G. Compton, *Sens. Actuators B* **2010**, *145*, 417–427; b) R. T. Kachoosangi, G. G. Wildgoose, R. G. Compton, *Anal. Chim. Acta* **2008**, *618*, 54–60; c) R. T. Kachoosangi, M. M. Musameh, I. Abu-Yousef, J. M. Yousef, S. M. Kanan, L. Xiao, S. G. Davies, A. Russell, R. G. Compton, *Anal. Chem.* **2009**, *81*, 435–442; d) K. Chaisiwamongkhol, K. Ngamchuea, C. Batchelor-McAuley, R. G. Compton, *Analyst* **2016**, *141*, 6321–6328.
[14] a) T. W. B. Lo, L. Aldous, R. G. Compton, *Sens. Actuators B* **2012**, *162*, 361–368; b) W. T. P. dos Santos, H. M. A. Amin, R. G. Compton, *Sens. Actuators B* **2019**, *279*, 433–439.
[15] P. Nayak, R.-C. Xie, R. G. Palgrave, R. G. Compton, *ChemElectroChem* **2021**, *8*, 911–917.
[16] a) X. Dai, O. Nekrassova, M. E. Hyde, R. G. Compton, *Anal. Chem.* **2004**, *76*, 5924–5929; b) X. Dai, R. G. Compton, *Analyst* **2006**, *131*, 516–521; c) A. L. Suherman, K. Ngamchuea, E. E. L. Tanner, S. V. Sokolov, J. Holter, N. P. Young, R. G. Compton, *Anal. Chem.* **2017**, *89*, 7166–7173.
[17] S. Eloul, R. G. Compton, *J. Phys. Chem. C* **2014**, *118*, 24520–24532.
[18] a) M. Pumera, *ACS Nano* **2014**, *8*, 7555–7558; b) S. V. Sokolov, S. Eloul, E. Kätelhön, C. Batchelor-McAuley, R. G. Compton, *Phys. Chem. Chem. Phys.* **2017**, *19*, 28–43; c) W. Cheng, R. G. Compton, *TrAC Trends Anal. Chem.* **2014**, *58*, 79–89.
[19] a) A. Aajoud, P. Ravanel, M. Tissut, *J. Agric. Food Chem.* **2003**, *51*, 1347–1352; b) N. Simon-Delso, V. Amaral-Rogers, L. P. Belzunces, J. M. Bonmatin, M. Chagnon, C. Downs, L. Furlan, D. W. Gibbons, C. Giorio, V. Girolami, D. Goulson, D. P. Kreutzweiser, C. H. Krupke, M. Liess, E. Long, M. McField, P. Mineau, E. A. D. Mitchell, C. A. Morrissey, D. A. Noome, L. Pisa, J. Settele, J. D. Stark, A. Tapparo, H. Van Dyck, J. Van Praagh, J. P. Van der Sluijs, P. R. Whitehorn, M. Wiemers, *Environ. Sci. Pollut. Res. Int.* **2015**, *22*, 5–34.
[20] A. S. Gunasekara, T. Truong, K. S. Goh, F. Spurlock, R. S. Tjeerdema, *J. Pestic. Sci.* **2007**, *32*, 189–199.
[21] N. Yildirim, G. Agar, *Toxicol. Ind. Health* **2015**, *32*, 1450–1455.
[22] a) C. Vidau, R. A. González-Polo, M. Niso-Santano, R. Gómez-Sánchez, J. M. Bravo-San Pedro, E. Pizarro-Estrella, R. Blasco, J.-L. Brunet, L. P. Belzunces, J. M. Fuentes, *Neurotoxicology* **2011**, *32*, 935–943; b) L. W. Pisa, V. Amaral-Rogers, L. P. Belzunces, J. M. Bonmatin, C. A. Downs, D. Goulson, D. P. Kreutzweiser, C. Krupke, M. Liess, M. McField, C. A. Morrissey, D. A. Noome, J. Settele, N. Simon-Delso, J. D. Stark, J. P. Van der Sluijs, H. Van Dyck, M. Wiemers, *Environ. Sci. Pollut. Res. Int.* **2015**, *22*, 68–102.
[23] J. L. Miller, T. S. Schmidt, P. C. Van Metre, B. J. Mahler, M. W. Sandstrom, L. H. Nowell, D. M. Carlisle, P. W. Moran, *Sci. Adv.* **2020**, *6*, eabc1299.
[24] C. C. Tingle, J. A. Rother, C. F. Dewhurst, S. Lauer, W. J. King, *Rev. Environ. Contam. Toxicol.* **2003**, 1–66.
[25] a) B. Morzycka, *J. Chromatogr. A* **2002**, *982*, 267–273; b) T. Wang, J. Hu, C. Liu, *Environ. Monit. Assess.* **2014**, *186*, 2767–2774; c) Y. Cheng, F. Dong, X. Liu, J. Xu, W. Meng, N. Liu, Z. Chen, Y. Tao, Y. Zheng, *Anal. Methods* **2014**, *6*, 1788–1795; d) X. Li, H. Li, W. Ma, Z. Guo, X. Li, S. Song, H. Tang, X. Li, Q. Zhang, *Food Chem.* **2019**, *281*, 85–90; e) R. Tomazini, G. M. Grosseli, D. N. R. de Sousa, P. S. Fadini, F. T. Saia, A. Langenhoff, B. van der Zaan, A. A. Mozeto, *Anal. Methods* **2020**, *12*, 3242–3249.
[26] a) N. Vasylieva, K. C. Ahn, B. Barnych, S. J. Gee, B. D. Hammock, *Environ. Sci. Technol.* **2015**, *49*, 10038–10047; b) Q. Tu, M. E. Hickey, T. Yang, S. Gao, Q. Zhang, Y. Qu, X. Du, J. Wang, L. He, *Food Control* **2019**, *96*, 16–21; c) R. H. O. Montes, R. M. Dornellas, L. A. J. Silva, A. L. Squissato, E. M. Richter, R. A. A. Munoz, *J. Solid State Electrochem.* **2016**, *20*, 2453–2459; d) F. Okumura, R. B. Amaral, E. Orestes, A. B. Silva, L. H. Mazo, *J. Braz. Chem. Soc.* **2016**, *27*, 925–932; e) M. Maulidiyah, T. Azis, L. Lindayani, D. Wibowo, L. O. A. Salim, A. Aladin, M. Nurdin, *J. Electrochem. Sci. Technol.* **2019**, *10*, 394–401; f) M. Nurdin, O. A. Prabowo, Z. Arham, D. Wibowo, M. Maulidiyah, S. K. M. Saad, A. A. Umar, *Surf. Interfaces* **2019**, *16*, 108–113; g) S. Kumar, N. Vasylieva, V. Singh, B. Hammock, S. G. Singh, *Electroanalysis* **2020**, *32*, 2056–2064; h) S. El-Akaad, M. A. Mohamed, M. M. Elmasri, N. S. Abdelwahab, E. A. Abdelaleem, S. De Saeger, N. Beloglazova, *J. Electrochem. Soc.* **2020**, *167*, 027543.
[27] C. Batchelor-McAuley, J. Ellison, K. Tschulik, P. L. Hurst, R. Boldt, R. G. Compton, *Analyst* **2015**, *140*, 5048–5054.
[28] R. R. Moore, C. E. Banks, R. G. Compton, *Anal. Chem.* **2004**, *76*, 2677–2682.
[29] a) Y. Y. Chan, A. Y. S. Eng, M. Pumera, R. D. Webster, *ChemElectroChem* **2015**, *2*, 1003–1009; b) K. Chaisiwamongkhol, C. Batchelor-McAuley, S. V. Sokolov, J. Holter, N. P. Young, R. G. Compton, *Appl. Mater. Res.* **2017**, *7*, 60–66.
[30] J. Ellison, C. Batchelor-McAuley, K. Tschulik, R. G. Compton, *Sens. Actuators B* **2014**, *200*, 47–52.
[31] a) M. A. Fryling, J. Zhao, R. L. McCreery, *Anal. Chem.* **1995**, *67*, 967–975; b) C. A. Thorogood, G. G. Wildgoose, A. Crossley, R. M. J. Jacobs, J. H. Jones, R. G. Compton, *Chem. Mater.* **2007**, *19*, 4964–4974; c) R. W. Murray, *Electroanal. Chem.* **1984**, *13*, 191; d) C. E. Banks, T. J. Davies, G. G. Wildgoose, R. G. Compton, *Chem. Commun.* **2005**, 829–841.
[32] M. Li, P. Li, L. Wang, M. Feng, L. Han, *J. Agric. Food Chem.* **2015**, *63*, 4435–4443.
[33] P. W. Atkins, J. De Paula, *Atkins' Physical Chemistry*, 9th ed., Oxford University Press, Oxford, **2010**.
[34] a) L. Chen, X. Li, E. E. L. Tanner, R. G. Compton, *J. Agric. Food Chem.* **2017**, *8*, 4771–4778; b) W. T. P. dos Santos, R. G. Compton, *Sens. Actuators B* **2019**, *285*, 137–144.
[35] S. S. Batsanov, *Inorg. Mater.* **2001**, *37*, 871–885.
[36] R. W. Murray, *Molecular design of electrode surfaces*, Wiley, New York, **1992**.
[37] a) H. Chang, A. J. Bard, *J. Am. Chem. Soc.* **1991**, *113*, 5588–5596; b) R. T. Kachoosangi, C. E. Banks, X. Ji, R. G. Compton, *Anal. Sci.* **2007**, *23*, 283–289; c) L. Xiao, E. J. F. Dickinson, G. G. Wildgoose, R. G. Compton, *Electroanalysis* **2010**, *22*, 269–276.
[38] a) X. Li, C. Batchelor-McAuley, K. Tschulik, L. Shao, R. G. Compton, *ChemPhysChem* **2015**, *16*, 2322–2325; b) X. Li, C. Lin, C. Batchelor-McAuley, E. Laborda, L. Shao, R. G. Compton, *J. Phys. Chem. Lett.* **2016**, *7*, 1554–1558.
[39] a) N. V. Rees, C. E. Banks, R. G. Compton, *J. Phys. Chem. B* **2004**, *108*, 18391–18394; b) C. E. Banks, N. V. Rees, R. G. Compton, *J. Phys. Chem. B* **2002**, *106*, 5810–5813.
[40] A. J. Bard, L. R. Faulkner, *Electrochemical Methods* **2001**, *2*, 580–632.
[41] R. G. Compton, C. E. Banks, *Understanding voltammetry*, Third ed., World Scientific Publishing Europe, London, **2018**.
[42] a) Y. Wang, L. Chen, K. Chaisiwamongkhol, R. G. Compton, *Food Chem.* **2020**, *309*, 125606; b) Y. Wang, L. Chen, R. G. Compton, *Food Chem.* **2020**, *323*, 126844; c) Y. Uchida, E. Kätelhön, R. G. Compton, *J. Electroanal. Chem.* **2019**, *848*, 113290; d) Y. Uchida, E. Kätelhön, R. G. Compton, *J. Electroanal. Chem.* **2019**, *835*, 60–66.

Manuscript received: May 20, 2021
Revised manuscript received: June 8, 2021
Accepted manuscript online: June 9, 2021